High-efficiency non-ablative UV laser nano-scale processing of fused silica by stable filamentation

BENEDIKT HERMANN, OLIVIER BERNARD, ^{iD} LUCA MUSCARELLA, AND YVES BELLOUARD[*] ^{iD}

Galatea Laboratory, École Polytechnique Fédérale de Lausanne (EPFL), Rue de la Maladiére 71b, CH - 2000 Neuchâtel, Switzerland
[*]*yves.bellouard@epfl.ch*

Abstract: Over the last decades, three-dimensional micro-manufacturing of fused silica via near-infrared ultrafast laser exposure combined with an etching step has become an established technique for producing complex three-dimensional components. Here, we explore the effect of ultraviolet exposure on process efficiency. Specifically, we demonstrate that shorter wavelengths not only enable enhanced resolution but also yield higher etching selectivity, with an order of magnitude lower pulse energy and significantly higher repetition rates than current practice. This result is obtained using an exposure regime where the laser beam alternates between regimes of self-focusing and defocusing in a stable manner, forming a localized filament. Using this principle, we demonstrate the fabrication of self-organized nano-channels with diameters as small as 120 nm after etching, reaching extreme aspect ratios, exceeding 1500.

1. Introduction

Ultrashort pulse lasers have proven to be versatile tools for numerous applications, notably in the field of glass micromachining. Peak optical intensities exceeding $GW\,cm^{-2}$ are nowadays routinely achieved by commercial ytterbium-based lasers generating sub-picosecond pulses. At such optical intensities, multiphoton absorption triggers intricate laser-matter interactions [1,2]. Thanks to the nonlinear nature of multiphoton absorption, the interaction volume can be confined within the focal spot of the laser, leading to potentially smaller-than-wavelength affected zones.

In fused silica, laser-induced modifications can take various forms, including locally densified volumes [3], self-organized nanogratings [4], or networks of nanopores [5]. Each of these laser-induced material transformations has been associated with unique applications, such as waveguides [3,6], chemically etcheable zones [7], zones with tuneable retardance [8] or stress [9,10]. In particular, this process enables free-form manufacturing of micro-mechanical glass devices for optical or medical applications, as well as precise fabrication of microfluidic chips [11]. Detailed studies on processing parameters have been conducted at near-infrared (NIR) wavelengths around λ = 1000 nm by various authors [12–14]. In [14], two regimes with enhanced etching have been identified [14]. Regime I, where etching is driven by defects, and regime II, where nanogratings are associated with the formation of etched channels. Regime I requires a limited pulse overlap of about >10 pulses/μm, whereas regime II requires higher pulse densities, typically >100 pulses/μm. Thermal accumulation [15,16] limits pulse repetition rates to around 1 MHz, depending on the pulse energy used. This value intrinsically limits the processing scanning speeds (typically to about 50 mm s^{-1}), and ultimately, the yield of the process.

In an attempt to improve the intrinsic yield of the process, here, we explore the effect of shorter laser wavelengths on bulk etching of fused silica. We use a high-power, frequency-tripled ytterbium-based laser (Tangor 100, Amplitude) operating at 343 and emitting pulses with a

duration of 450 fs. The shorter wavelength facilitates multiphoton ionization, since fewer photons are required to overcome the band gap of approximately 9 eV in fused silica. Consequently, we expect a lower threshold for nonlinear modification using ultra-violet (UV) laser pulses.

The critical power (P_{crit}) required for Kerr-lensing, inducing a nonlinear index n_2, is proportional to the square of the wavelength: $P_{\mathrm{crit}} = \alpha\lambda^2/(4\pi n n_2)$ [17], where n denotes the refractive index of the material, and α accounts for the original beam shape. Thus, filamentation and self-focusing are expected to play important roles at lower pulse energies for UV than for NIR beams, which affects the deposition and distribution of laser-induced modifications.

Our experiments with a UV femtosecond laser show self-arranged sub-micrometer-sized circular channels within the laser-affected zone, which have an improved etching rate (20% higher than for NIR). As lower pulse energies are used, thermal effects occur at higher laser repetition rates for UV. Up to 2MHz (i.e., the upper repetition rate limit of our laser system), we do not observe cumulative effects detrimental for etching. These findings help to further improve laser-assisted etching of fused silica in terms of achievable aspect ratio, etching rate, and process yield. In the sequel, we demonstrate the high etching selectivity of UV-laser-exposed zones under certain exposure parameters, along with a detailed analysis of the laser-induced microstructures. Finally, we discuss the formation of a stable self-focusing/defocusing regime at the origin of the etching enhancement.

2. Method

A reflective objective coated with a reflective-UV-enhancing aluminum layer focuses the laser pulses. The broadband reflectivity of the aluminum coating allows us to use the objective for both studied wavelengths (1030 nm and 343 nm), to compare them under the same focusing conditions. The entrance pupil of the objective has a diameter of 8.4 mm. At this location, the beam had a diameter, defined by the $1/e^2$ width of 7.0 mm, which results in an effective numerical aperture of $\mathrm{NA}_e = 0.16$. As a first approximation, the focal spot size (waist radius w_0) as a function of wavelength (λ) can be estimated from Gaussian beam equations $w_0 = \frac{\lambda}{\mathrm{NA}_e\pi}$. A reflective objective obscures the central area of the beam (Cassegrain-type Schwarzschild design), resulting in annular focusing conditions. Supplement 1 S1 provides the simulated beam profiles for these focusing conditions, see Fig. S1. We used Fresnel integration to simulate the intensity profile around the focal plane, and neglected spherical aberrations caused by the air-glass interface as we work with moderate focusing angles ($\mathrm{NA}_e = 0.16$).

To test the role of focusing conditions, we compare the results obtained with a standard transmission objective. This objective has surface coatings for UV, and a stronger diffraction-limited focusing power of 0.38NA. The pulse density along a written track in fused silica is given by: $\rho = f/v$, where f is the pulse repetition rate. The dose per pulse delivered to the material is $\phi = E_p\rho/w_0$. The repetition rate is kept constant at 200 kHz, except for the study of cumulative thermal effects. Fused silica samples (Corning 7980 0F) are translated through the focus at a depth of 200 μm with two-dimensional translation stages reaching velocities up to 300 mm s^{-1}, after a maximum acceleration length of 30 mm.

After the inscription of line patterns with varying velocities and laser parameters, the samples are sliced with a diamond wire saw and polished, before chemical etching. In this study, we compare two etchants: hydrofluoric acid (HF, 2.5wt% in water at room temperature) and sodium hydroxide (NaOH, 5wt% in water at 80°C). The length of the etched lines is extracted from bright-field microscope images, with an image-processing algorithm using gradients in the direction perpendicular to the lines and intensity thresholds. Figure 1 provides an illustration of detected lines from a microscope image.
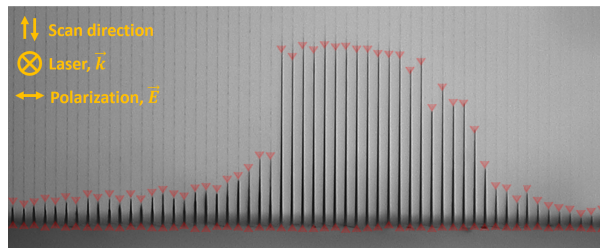
Fig. 1. Microscope image of UV-written lines, etched in a static bath of HF (5 wt% aqueous solution at room temperature) for 4 h. The length of each line is determined by our image-processing algorithm, indicated here by red triangles. The displayed set contains a scan of the pulse density ρ from 20 μm^{-1} to 40 μm^{-1} (left to right). The pulse energy is $E_p = 200$ nJ for all tracks displayed. The line spacing is 25 μm.

3. Results

3.1. Etching results

Initially, a wide scan of the laser pulse energy (E_p), and pulse density along the writing track (ρ) was performed for the NIR and UV wavelengths using the reflective objective. The polarization was kept perpendicular to the writing direction. Measured etching rates in hydrofluoric acid (HF) for NIR-written lines are in line with the behavior observed in Ref. [14]. The many pulses regime, where nanogratings enhance etching, and the few pulse regime, where chemical defects do, are both highlighted in Fig. 2. The UV-written lines show significantly different etching behavior. First, the pulse energy threshold for the etching process to start is about eight times lower. A surprisingly narrow region of fast etching rate is observed at a low pulse density of around 9 μm^{-1}. This regime seems to be rather independent of the pulse energy, in particular in the region between 100 nJ and 300 nJ. To better characterize this regime, we repeat the etching test with a narrower parameter scan, see Fig. 3. The results indicate that only ρ within 8 μm^{-1} to 10 μm^{-1} achieves a high etching rate. We refer to this region as UV-I. A similar pattern is recovered when using the transmission objective with a stronger focusing power of 0.38 NA, see Supplement 1 Fig. S2. A consistency test carried out for $E_p = 200$ nJ with six repetitions in both writing directions, confirms a constant etching rate of 100 μm h^{-1} within regime UV-I. The steep cut-offs on both sides of the plateau are highly repeatable. From this data set, we deduce an uncertainty of the etching rates including statistical variations in the order of 5 μm h^{-1} in regime UV-I.

3.2. Effect of polarization

The effect of polarization is known to play an important role in the mechanism behind the formation of nanogratings in fused silica: they appear perpendicularly to the laser polarization [4]. This results in a highly polarization-sensitive etching rate for this regime [18]. An insensitivity to polarization in the few-pulses regime has been reported recently for NIR wavelengths [19,20]. With ultrafast UV pulses, in regime UV-I, efficient etching appears for both perpendicular and parallel polarization. However, for parallel polarization, fast etching rates occur for a significantly smaller window of pulse densities (Fig. 4).

3.3. Cumulative effects

For the purpose of studying effects occurring at high repetition rates, allowing heat to accumulate locally, we perform the track-etching experiment with varying pulse repetition rates. To keep the pulse density constant, the velocity of the stage is adjusted accordingly. Figure 5 shows the
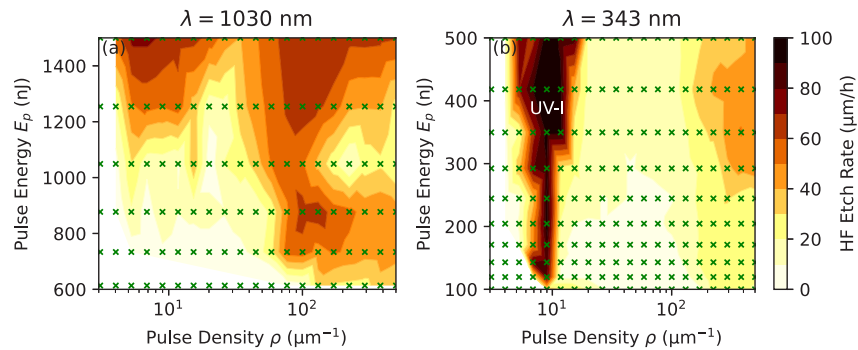
Fig. 2. Filled contour plots of the etching rates in HF for lines written with NIR (a) and UV (b) as a function of pulse energy E_p and pulse density ρ. Green crosses indicate measured data points of the two-dimensional parameter scan. The color scale is identical for both plots.
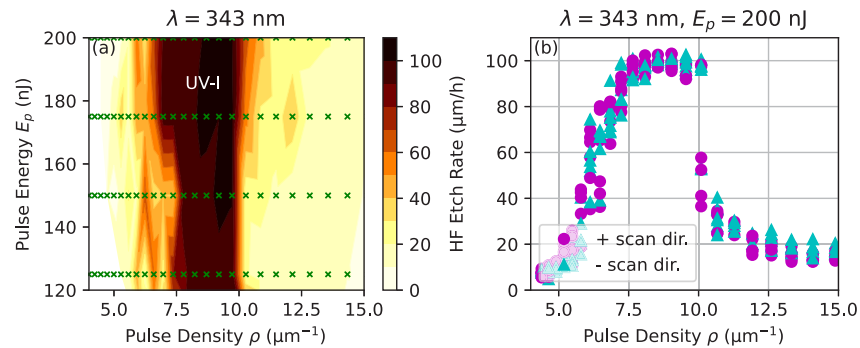

Fig. 3. (a) High-resolution scan of etching rates in HF for machining parameters pulse energy E_p and pulse density ρ with perpendicular polarization. (b) Repeatability study for $E_p = 200$ nJ and both writing directions.
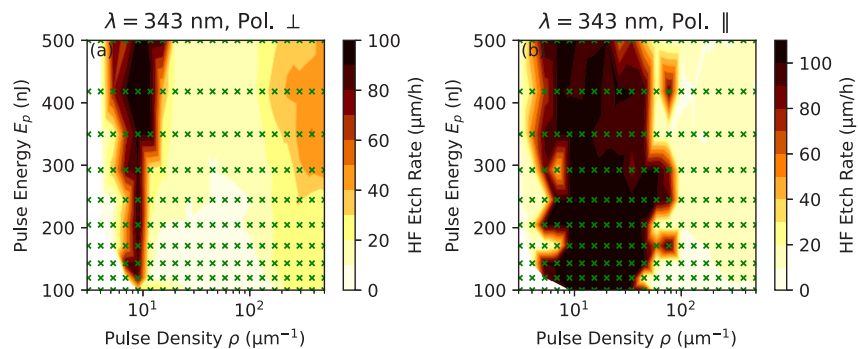

Fig. 4. Comparison of the HF etching rate for both linear laser polarization states. (a) Perpendicular polarization. For easier comparison, we show again the data of Fig. 2(b). (b) Parallel polarization. A much wider parameter range of pulse densities enables high etching rates.

etching rate for NIR- and UV-written lines for selected pulse energies. We observe a degradation of the etching rate for NIR-written lines with repetition rates above 500 kHz. Heat accumulation leads to a local temperature increase, above the softening temperature of fused silica of around 1600°C. This triggers the formation of bubbles shown in the inset of Fig. 5. Bubbles emerge from local transient heating, which may fill up the nanostructures that enable efficient etching. This observation is in agreement with previous studies concerning the cumulative regime of ultrafast modification in fused silica at NIR wavelengths [21]. For UV-written lines, we do not observe a degradation of the etching process with repetition rates lower than 2. Higher values could not be tested with the present amplifier system. Heat might as well accumulate in regime UV-I at higher rates, but due to the lower pulse energy and more efficient absorption, the temperature does not overcome the melting point. We elaborate further on this aspect and the consequences for rapid pattern inscription for micromanufacturing in the discussion.
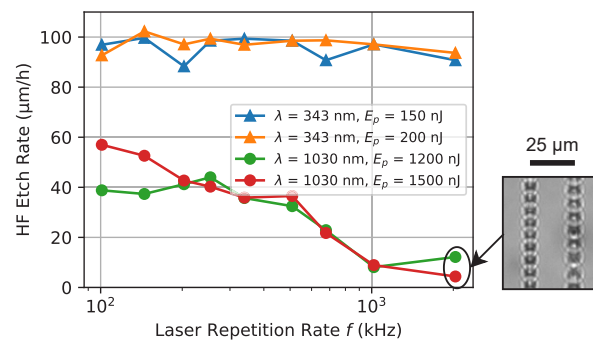

Fig. 5. Etching rate in HF as a function of laser repetition rate (f) for NIR- and UV-written lines with 10 pulses/μm . For UV, an order of magnitude less pulse energy is required to produce tracks which are etching 50% faster. The inset shows a micrograph of self-organized periodic bubble formation, obtained with NIR exposure at $f = 2$ MHz.

3.4. Effect of annealing and selection of etchant

Insights into the driving mechanism of the etching process can be obtained through variations of the chemical etchant, and from annealing at different temperatures before etching [14]. Here, we compare acidic (HF, 5 wt% aqueous solution at room temperature), and alkaline (sodium hydroxide NaOH, 5 wt% in water at 80°C) solutions. We tested annealing temperatures of 300°C and 600°C for a duration of 10 h before the etching process. The results of all combinations of annealing temperatures and etchants are reported in Fig. 6. With NaOH, an etching rate of 380 $\mu m\,h^{-1}$ is observed prior to annealing, almost four times faster than with HF. For HF, the etching rate is not affected by an annealing temperature of 300°C. A drop of a few percent is observed for elevated annealing at 600°C. For NaOH, the drop in etching rate after annealing is significantly larger: at 300°C, the etching rate drops by 25%, and at 600°C, it decreases by about 45%.

3.5. Cross-section of etched channels

The shape of the cross-section ultimately defines the smallest feature size of etched parts. We characterize the cross-sections of UV-written lines with a scanning electron microscope (SEM, JEOL JSM-7500 TFE, operated at 5 kV). For low pulse density of $\rho = 4$ μm^{-1}, where the etching rate is slow (<5 μm h^{-1}), the cross-section after etching in HF for 4 h appears to be a homogeneous ellipse, elongated along the laser propagation direction, see Fig. 7(a). This modification is about 30 μm-long on the laser propagation direction: Kerr-lensing extends the
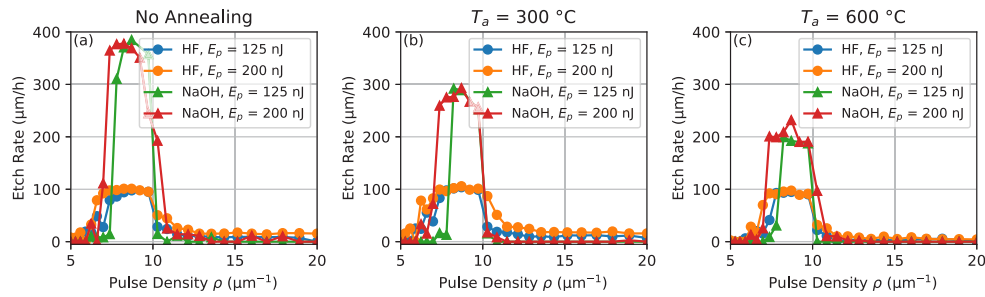
Fig. 6. Comparison of etching rates for HF and NaOH. The three sub-plots correspond to three different annealing scenarios: no annealing, 300 °C, and 600 °C. The samples were heated for a duration of 10 h.

affected volume compared to the expected focal volume (see Fig. S1a). Note that unetched channels are not visible with this method.
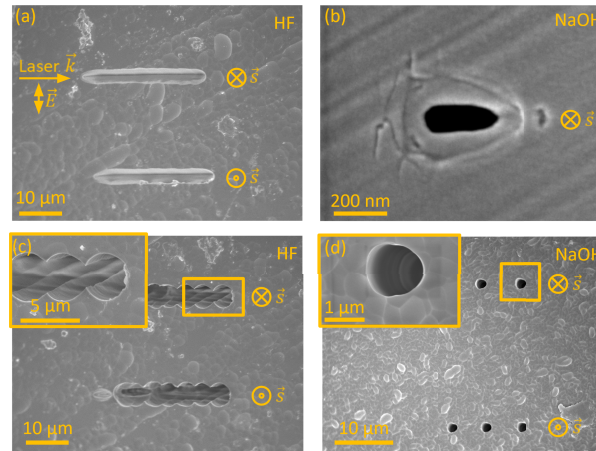

Fig. 7. SEM images of etched cross-sections. Two lines with opposite writing directions and otherwise equal machining parameters are shown per image. (a) Pulse energy: $E_p = 200$ nJ, pulse overlap: $\rho = 4.0$ μm^{-1}, HF for 4 h at 20 °C. Here, almost no etching is observed. (b) Pulse energy: $E_p = 100$ nJ, pulse overlap: $\rho = 9.2$ μm^{-1}, NaOH for 0.5 h at 90 °C. A single channel is etched. Note the smaller scale. (c) Pulse energy: $E_p = 200$ nJ, pulse overlap: $\rho = 9.2$ μm^{-1}, HF for 4 h at 20 °C. Series of transversely connected channels with high etching rate. (d) Pulse energy: $E_p = 110$ nJ, pulse overlap: $\rho = 9.2$ μm^{-1}, NaOH for 4 h at 90 °C. Several well-separated channels appear, highlighting the selectivity of NaOH for such modifications. Images (c) and (d) are taken with an observation angle relative to the surface of approximately 10°, to reveal the inner walls of the etched channels. For all images, the laser propagates from left to the right ($\vec{k}$), and is scanned perpendicularly to the polished surface ($\vec{s}$). The laser is polarized perpendicularly to the scanning direction ($\vec{E}$).

The cross-section for regime UV-I (fast etching, pulse densities of around 9 μm^{-1}), consists of single (see Fig. 7(b)) or multiple periodically arranged channels (see Figs. 7(c),(d)) along the laser propagation direction. The originally elliptical cross-section develops into a circular shape during the etching process. Individual channels may overlap and form a connected cavity (Fig. 7(d)).

Compared to HF, NaOH provides a higher etching selectivity, as the etching rate of pristine fused silica is about 10 times slower. The cross-section for lines etched for 4 in NaOH at 90°C shows disconnected, yet periodically arranged spherical channels with diameters of about 1.2 μm (see Fig. 7(c)). The number of channels increases with laser pulse energy. With pulse energies ranging from 100 nJ to 200 nJ, we observe either single channels, or up to six periodically arranged channels along the propagation axis. We observe the same behavior for these types of modifications using a 0.38 NA transmission objective lens instead of the reflective Schwarzschild objective. A single pore channel etched for 0.5 h in NaOH is depicted in detail in Fig. 7(b). The SEM image reveals an elliptical cross-section of 120 nm × 320 nm, elongated along the laser propagation direction. We quantify the aspect ratio of the channel by the ratio of its cross-section diameter to its length. The diameter is obtained from an SEM image, whereas the length is estimated from the etching rate obtained with optical microscopy. The aspect ratio of the channel presented in Fig. 7(b), along its narrow direction, is about 1600. The etched zone is surrounded by a shell which we attribute to a high-pressure shock wave, that seems to share morphological similarities with nanostructures reported in sapphire under tight focusing [22]. Direct-write channels with strongly asymmetric cross-sections of 40 nm × 1400 nm were demonstrated using a strong focusing regime (1.1 NA) and a 100 fs NIR laser [23]. Bessel beams have been used to produce sub- holes elongated along the laser propagation direction on the surface of fused silica [24,25] and in optical fibers [26].

3.6. Raman spectroscopy

To better understand the nature of the UV femtosecond modifications and the formation of the systematically arranged channels in the fast-etching regime, we perform micro-Raman spectroscopy of modified zones ($\lambda_{Raman} = 532$ nm, $NA_{Raman} = 0.6$). The raw data, depicted in Fig. 8, corresponds to a line written with a pulse density of 4.0 μm^{-1} and a pulse energy of 200 nJ. A local rise of the D2-peak at 606 μm^{-1} within the modified area is visible. A similar rise of the D2-peak has been attributed to an increase of three-membered ring structures in the fused silica matrix, causing densification and increase in refractive index [27–31].
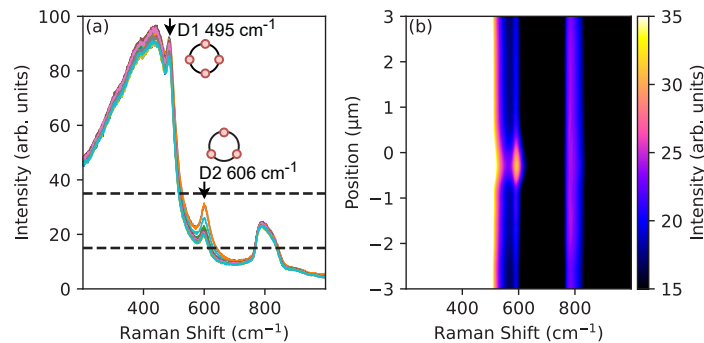

Fig. 8. Micro-Raman spectroscopy measurements. The probe beam is scanned over the polished cross-section of a track written with a low pulse density of 4.0 μm^{-1}. (a) Raman spectra obtained during the scan. (b) Raman spectral map, with the shift reported on the x-axis, and the distance from the femtosecond laser-exposed track on the y-axis. The increase of the D2-peak in modified regions corresponds to an increase of three-membered Si-O rings leading to densification. The dashed lines in (a) indicate the range of the color scale used in (b).

4.   Discussion

A machining regime for laser-assisted etching of fused silica using 450 fs-long laser pulses at 343 nm has been reported and characterized. The main experimental observations in this study are summarized below.

- In regime UV-I, corresponding to pulse densities around 9 μm^{-1}, etching rates up to 380 μm/h are achieved in an aqueous solution of NaOH. This is about 20% faster than observed in a previous study with NIR wavelengths [14].

- For comparable focusing conditions and pulse durations, cumulative effects for NIR pulses start to hinder the etching for laser repetition rates above 500 kHz, whereas for UV pulses, no significant drop of etching rate is observed up to 2 MHz, the maximum rate tested in this study. As a consequence, laser machining with at least five times higher translation speed (exceeding 250 mm/s) is possible in regime UV-I.

- Annealing tests reveal a decay of the etching rate by 45% for NaOH when the sample is heated to 600°C before etching. This indicates that chemical defects enhance the etching rate, but morphological changes surviving the annealing step are another key aspect of the etching process.

- The cross-section of etched channels consists of tunnels, with sub-micron cross-sections, periodically arranged along the laser propagation direction. The number of tunnels can be tuned from one to six for pulse energies from 100 nJ to 200 nJ. A single tunnel has a diameter of 120 nm after etching for 0.5 h in NaOH. Thanks to the high etching selectivity, the aspect ratio of this tunnel reaches about 1600. A further increase of pulse energy leads to a less regular formation of pores, which we attribute to the strongly non-linear laser-plasma interaction for pulse energies far above the modification threshold.

For low pulse densities around 4 μm^{-1}, we find non-etchable densified regions with high homogeneity. Such modifications might be suitable for fabricating direct-write waveguides, at high processing speeds in the order of 1 m s^{-1}. Waveguide inscription in fused silica with NIR pulses requires pulses shorter than 100 fs, and needs high pulse densities to achieve a significant refractive index change. This leads to slow scanning speeds in the order of 1 mm/s, which is a limiting factor for industrial applications. We explain the transition from a homogeneous modulation of refractive index to self-arranged etching channels by increasing the laser pulse density with the following phenomenological model, as illustrated by Fig. 9. Fused silica has a nonlinear refractive index of about 2.5×10^{-20} m^2/W at UV wavelengths [32], and a refractive index at 343 nm of 1.4781 [33], the critical pulse power is P_{crit} = 465 kW [34]. For our laser pulse duration of 450 fs, the critical pulse energy for Kerr-lensing is $E_{crit} = P_{crit}/\tau_p$ = 209 nJ. At pulse energies around this value, and low pulse densities (<5 μm^{-1}), the laser-affected volume is extended by Kerr-lensing, leading to the formation of an elongated, homogeneously densified zone (see Fig. 7(a) and Fig. 8).

At higher pulse densities ($\gtrsim$ 8 μm^{-1}), the laser-induced refractive index increases and affects subsequent laser pulses, affecting their focusing conditions. The result is an amplified self-focusing behavior, that creates highly localized intensity peaks. Kerr-lensing certainly still affects the focusing properties of each individual pulse, regardless of the state of the material being exposed. We do not observe hot spots for low pulse densities, hence, there is a dependence on the local condition of the material to generate such channels. The laser-induced local increase in refractive index causes refocusing of the subsequent pulses, forming intensity peaks. In these peaks, molecular defects and pores appear. Once pores appear, field enhancement increases further the energy absorption. Laser-induced refractive index modulation, Kerr-lensing, and field enhancement interplay into forming regular and well-connected pores and defects (channel
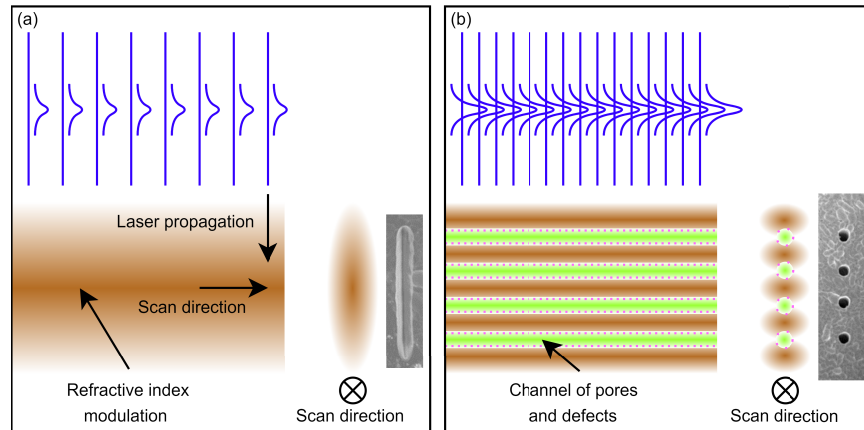
Fig. 9. Phenomenological model of the formation of self-arranged periodic sub–scale channels in UV-written tracks. Low pulse densities (left) generate a smooth refractive index modulation. With higher pulse density (right), the refractive index modulation is intense enough to create intermittent strong foci along the laser propagation direction. These hot spots lead to the formation of pores and defects.

or groove). This interaction requires reaching a critical pulse density, here $\gtrsim 8\ \mu m^{-1}$. If the pulse density is too high, the increase in field enhancement results in an unstable and chaotic formation of pores. The loss of connectivity explains the sharp drop observed in the etching rate for pulse densities exceeding $10\ \mu m^{-1}$. This drop is even more pronounced for NaOH than for HF, due to the slower etching rate of pristine fused silica of NaOH. This supports the relevance of connectivity of pores to achieve high etching rates, through percolation. The laser polarization parallel to the writing direction enhances the connectivity resulting in a wider range of etchable writing velocities (see Fig. 4).

When using a transmission objective (0.38 NA), the fast-etching regime UV-I and the formation of circular channels are recovered. This indicates that both focusing conditions (Schwarzschild reflective objective 0.23 NA and transmission objective 0.38 NA) behave similarly. We conclude that Kerr-lensing and laser-induced modulation of the refractive index around the waist are the driving factors toward these modifications. Focusing conditions play here a less important role.

Self-arranged patterns have been observed in crystalline dielectrics (lithium niobate) through modification by a strongly focused IR laser (NA: 0.65) [35]. In this study, the self-arrangement is explained by interference patterns along the laser propagation through reflection at the focal plasma, and smaller transverse patterns are attributed to plasmonic resonances at the plasma-to-dielectric interface.

5. Conclusions

UV femtosecond lasers provide an efficient tool for rapid micro- and nano-processing of fused silica through chemical etching. High writing velocities of several 100 mm/s are achieved thanks to the low pulse overlap in combination with high laser pulse repetition rates, with yet low-pulse energies. The shape of single laser tracks is affected by alternating self-focusing/defocusing phenomena (filamentation), which are remarkably stable and reproducible when appropriate machining parameters are applied. The cross-sections of etched tracks exhibit single or multiple equally spaced nano-pores, with diameters down to 100 nm and aspect ratios exceeding 1500. The number of pores per track is governed by the laser pulse energy.

Supplemental document. See Supplement 1 for supporting content.

References

1. D. Du, X. Liu, G. Korn, J. Squier, and G. Mourou, "Laser-induced breakdown by impact ionization in SiO2 with pulse widths from 7 ns to 150 fs," Appl. Phys. Lett. **64**(23), 3071–3073 (1994).
2. B. C. Stuart, M. D. Feit, A. M. Rubenchik, B. W. Shore, and M. D. Perry, "Laser-induced damage in dielectrics with nanosecond to subpicosecond pulses," Phys. Rev. Lett. **74**(12), 2248–2251 (1995).
3. K. M. Davis, K. Miura, N. Sugimoto, and K. Hirao, "Writing waveguides in glass with a femtosecond laser," Opt. Lett. **21**(21), 1729–1731 (1996).
4. Y. Shimotsuma, P. G. Kazansky, J. Qiu, and K. Hirao, "Self-organized nanogratings in glass irradiated by ultrashort light pulses," Phys. Rev. Lett. **91**(24), 247405 (2003).
5. M. Sakakura, Y. Lei, L. Wang, Y.-H. Yu, and P. G. Kazansky, "Ultralow-loss geometric phase and polarization shaping by ultrafast laser writing in silica glass," Light: Sci. Appl. **9**(1), 15 (2020).
6. K. Miura, J. Qiu, H. Inouye, T. Mitsuyu, and K. Hirao, "Photowritten optical waveguides in various glasses with ultrashort pulse laser," Appl. Phys. Lett. **71**(23), 3329–3331 (1997).
7. A. Marcinkevičius, S. Juodkazis, M. Watanabe, M. Miwa, S. Matsuo, H. Misawa, and J. Nishii, "Femtosecond laser-assisted three-dimensional microfabrication in silica," Opt. Lett. **26**(5), 277–279 (2001).
8. E. Bricchi, B. G. Klappauf, and P. G. Kazansky, "Form birefringence and negative index change created by femtosecond direct writing in transparent materials," Opt. Lett. **29**(1), 119–121 (2004).
9. A. Champion, M. Beresna, P. Kazansky, and Y. Bellouard, "Stress distribution around femtosecond laser affected zones: effect of nanogratings orientation," Opt. Express **21**(21), 24942–24951 (2013).
10. Y. Bellouard, A. Champion, B. McMillen, S. Mukherjee, R. R. Thomson, C. Pépin, P. Gillet, and Y. Cheng, "Stress-state manipulation in fused silica via femtosecond laser irradiation," Optica **3**(12), 1285–1293 (2016).
11. Y. Bellouard, A. Said, M. Dugan, and P. Bado, "Fabrication of high-aspect ratio, micro-fluidic channels and tunnels using femtosecond laser pulses and chemical etching," Opt. Express **12**(10), 2120–2129 (2004).
12. S. Kiyama, S. Matsuo, S. Hashimoto, and Y. Morihira, "Examination of etching agent and etching mechanism on femotosecond laser microfabrication of channels inside vitreous silica substrates," J. Phys. Chem. C **113**(27), 11560–11566 (2009).
13. C. A. Ross, D. G. MacLachlan, D. Choudhury, and R. R. Thomson, "Optimisation of ultrafast laser assisted etching in fused silica," Opt. Express **26**(19), 24343–24356 (2018).
14. E. Casamenti, S. Pollonghini, and Y. Bellouard, "Few pulses femtosecond laser exposure for high efficiency 3d glass micromachining," Opt. Express **29**(22), 35054–35066 (2021).
15. C. B. Schaffer, J. F. García, and E. Mazur, "Bulk heating of transparent materials using a high-repetition-rate femtosecond laser," Appl. Phys. A **76**(3), 351–354 (2003).
16. S. M. Eaton, H. Zhang, P. R. Herman, F. Yoshino, L. Shah, J. Bovatsek, and A. Y. Arai, "Heat accumulation effects in femtosecond laser-written waveguides with variable repetition rate," Opt. Express **13**(12), 4708–4716 (2005).
17. G. Fibich and A. L. Gaeta, "Critical power for self-focusing in bulk media and in hollow waveguides," Opt. Lett. **25**(5), 335–337 (2000).
18. C. Hnatovsky, R. S. Taylor, E. Simova, V. R. Bhardwaj, D. M. Rayner, and P. B. Corkum, "Polarization-selective etching in femtosecond laser-assisted microfluidic channel fabrication in fused silica," Opt. Lett. **30**(14), 1867–1869 (2005).
19. M. Ochoa, P. Roldán-Varona, J. F. Algorri, J. M. López-Higuera, and L. Rodríguez-Cobo, "Polarisation-independent ultrafast laser selective etching processing in fused silica," Lab Chip **23**(7), 1752–1757 (2023).
20. O. Bernard, A. Kraxner, A. Boukhayma, J. A. Squier, C. Enz, and Y. Bellouard, "Third-harmonic generation monitoring of femtosecond-laser-induced in-volume functional modifications," Optica **10**(6), 774–782 (2023).
21. S. Rajesh and Y. Bellouard, "Towards fast femtosecond laser micromachining of fused silica: The effect of deposited energy," Opt. Express **18**(20), 21490–21497 (2010).
22. S. Juodkazis, K. Nishimura, S. Tanaka, H. Misawa, E. G. Gamaly, B. Luther-Davies, L. Hallo, P. Nicolai, and V. T. Tikhonchuk, "Laser-induced microexplosion confined in the bulk of a sapphire crystal: Evidence of multimegabar pressures," Phys. Rev. Lett. **96**(16), 166101 (2006).
23. Y. Liao, Y. Cheng, and C. Liu, *et al.*, "Direct laser writing of sub-50 nm nanofluidic channels buried in glass for three-dimensional micro-nanofluidic integration," Lab Chip **13**(8), 1626–1631 (2013).
24. F. Courvoisier, P.-A. Lacourt, M. Jacquot, M. Bhuyan, L. Furfaro, and J. Dudley, "Surface nanoprocessing with nondiffracting femtosecond bessel beams," Opt. Lett. **34**(20), 3163–3165 (2009).

25. M. Bhuyan, F. Courvoisier, P. Lacourt, M. Jacquot, R. Salut, L. Furfaro, and J. Dudley, "High aspect ratio nanochannel machining using single shot femtosecond bessel beams," Appl. Phys. Lett. **97**(8), 081102 (2010).
26. K. M. Aghdami, A. Rahnama, E. Ertorer, and P. R. Herman, "Laser nano-filament explosion for enabling open-grating sensing in optical fibre," Nat. Commun. **12**(1), 6344 (2021).
27. F. Galeener, "Planar rings in glasses," Solid State Commun. **44**(7), 1037–1040 (1982).
28. J. W. Chan, T. Huser, S. Risbud, and D. M. Krol, "Structural changes in fused silica after exposure to focused femtosecond laser pulses," Opt. Lett. **26**(21), 1726–1728 (2001).
29. L. Skuja, M. Hirano, H. Hosono, and K. Kajihara, "Defects in oxide glasses," phys. stat. sol. (c) **2**, 15–24 (2005).
30. C. W. Ponader, J. F. Schroeder, and A. M. Streltsov, "Origin of the refractive-index increase in laser-written waveguides in glasses," J. Appl. Phys. **103**(6), 063516 (2008).
31. J. Hernandez-Rueda, J. Clarijs, D. van Oosten, and D. M. Krol, "The influence of femtosecond laser wavelength on waveguide fabrication inside fused silica," Appl. Phys. Lett. **110**(16), 161109 (2017).
32. D. Milam, "Review and assessment of measured values of the nonlinear refractive-index coefficient of fused silica," Appl. Opt. **37**(3), 546–550 (1998).
33. I. H. Malitson, "Interspecimen comparison of the refractive index of fused silica*," J. Opt. Soc. Am. **55**(10), 1205–1209 (1965).
34. R. W. Boyd, *Nonlinear Optics* (Third Edition) (Academic Press, 2008).
35. S. Kudryashov, A. Rupasov, M. Kosobokov, A. Akhmatkhanov, G. Krasin, P. Danilov, B. Lisjikh, A. Abramov, E. Greshnyakov, E. Kuzmin, M. Kovalev, and V. Shur, "Hierarchical multi-scale coupled periodical photonic and plasmonic nanopatterns inscribed by femtosecond laser pulses in lithium niobate," Nanomaterials **12**(23), 4303 (2022).